TYPE IA SUPERNOVAE AND CHEMICAL EVOLUTION OF GALAXIES

K. NOMOTO, C. KOBAYASHI, H. UMEDA
Department of Astronomy & Research Center for the Early Universe, School of Science, University of Tokyo, Bunkyo-ku, Tokyo 113-0033, Japan

Abstract. The cosmic/galactic chemical evolutions have been modeled with the early metal enrichment by Type II supernovae (SNe II) and the delayed enrichment of Fe by Type Ia supernovae (SNe Ia). However, the exact nature of SN Ia progenitors have been obscure. Here we present the currently most plausible scenario of the progenitor binary systems of SNe Ia. This scenario involves strong winds from accreting white dwarfs, which introduces important metallicity effects, namely, low-metallicity inhibition of SNe Ia. Resultant predictions for the Galactic/cosmic chemical evolution and the cosmic SNe Ia rate are presented. Another importance of identifying the SN Ia progenitors lies in the use of SNe Ia as a "standard candle" to determine cosmological parameters. To examine whether the "evolution" of SNe Ia with redshift and metallicity is significant, we discuss how the metallicity affects the properties of the C+O white dwarfs such as the C/O ratio, and find the metallicity dependence is rather weak.

1. Introduction

There exist two distinct types of supernova explosions: One is Type II supernovae (SNe II), which are the core collapse-induced explosions of short-lived massive stars ($\gtrsim 8M_\odot$) and produce more O and Mg relative to Fe (i.e., [O/Fe] > 0). The other is Type Ia supernovae (SNe Ia), which are the thermonuclear explosions of accreting white dwarfs (WDs) in close binaries and produce mostly Fe and little O (e.g., Arnett 1996; Ruiz-Lapuente et al. 1997; Nomoto et al. 1994, 1997a). To construct chemical evolution models of galaxies, currently most crucial is to identify the exact progenitor binary systems of SNe Ia.

K. Nomoto and J.W. Truran (eds.), Cosmic Chemical Evolution, 33–46.

Another issue is the application of SNe Ia in cosmology (Branch 1998). Relatively uniform light curves and spectral evolution of SNe Ia have led to the use of SNe Ia as a "standard candle" to determine cosmological parameters, such as the Hubble constant, the density parameter, and the cosmological constant (Perlmutter et al. 1997; Schmidt et al. 1998). However, SNe Ia are not perfect standard candles but show some variations in their absolute magnitudes, light curve shapes, and spectra (e.g., Phillips 1993; Riess et al. 1998). It is important to understand the source of these variations and the dependence on the metallicity in order to use high-redshift SNe Ia for determining the cosmological parameters. The C/O ratio in the SNe Ia progenitors (C-O white dwarfs) may be related to this variation (Höflich et al. 1998; Umeda et al. 1998).

Here we first summarize the effects of stellar mass (M) and metallicity (Z) on the C/O ratio and its distribution in the C-O WDs (§2). We describe currently most plausible model of the SNe Ia progenitors, and introduce a metallicity dependent occurrence of SNe Ia (§3-4). In modeling the galactic/cosmic chemical evolution, this SN Ia model provides a new interpretation of the evolutionary change in [O/Fe] in the solar neighborhood and the SN II-like abundance patterns of the Galactic halo and the damped Lyα systems (§5-6). The metallicity dependent model of SNe Ia provides a testable prediction of cosmic supernova rates (§7).

2. C/O Ratios in White Dwarfs and Metallicity Effects

Umeda et al. (1998) calculated the evolution of intermediate-mass ($3-9M_\odot$) stars for metallicity Z=0.001 – 0.03. Figure 1 shows abundances in mass fraction in the inner core of the 6 $M_\odot$ star for $Y = 0.2775$ and $Z = 0.02$ at the end of the second dredge-up. It is seen that the central part of these stars is oxygen-rich. The C/O ratio is nearly constant in the innermost region, which was a convective core during He burning. Outside this homogeneous region, where the C-O layer grows due to He shell burning, the C/O ratio increases up to C/O $\gtrsim 1$; thus the oxygen-rich core is surrounded by a shell with C/O $\gtrsim 1$. In fact this is a generic feature in all the calculated models. The C/O ratio in the shell is C/O $\simeq 1$ for the star as massive as $\sim 7M_\odot$, and C/O > 1 for less massive stars (Fig. 1).

Figure 2 shows the central C/O ratio in mass fraction, which is not a monotonic function of the metallicity and the ZAMS mass. Two tendencies of the central C/O ratio can be noticed: (1) For a fixed Z, as stellar mass increases, the C/O ratio at the stellar center first increases to the maximum and then decreases. (2) For larger Z, the above maximum C/O ratio is larger. One reason for this complexity is that the C/O ratio is sensitive to the evolutionary change in the convective core size during the later stage

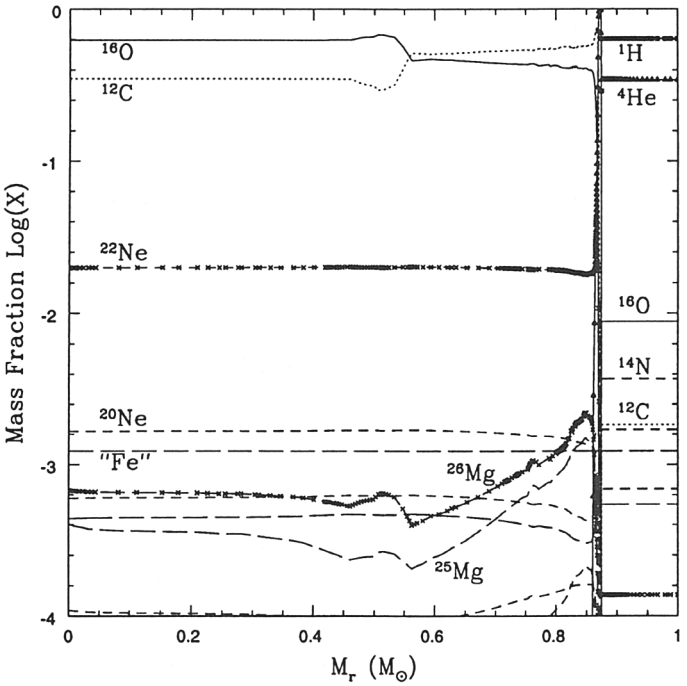

Figure 1. Abundances in mass fraction in the inner core of the 6 $M_\odot$ star for $Y = 0.2775$ and $Z = 0.02$ at the end of the second dredge-up (Umeda et al. 1998).

of He burning. Small differences in the core temperature and opacity lead to a different evolutionary behavior of the convective core, which largely changes the C/O ratio.

If the $3 - 9M_\odot$ star is a primary star in a close binary system, it forms a C+O WD, which in some cases can evolve to a thermonuclear supernova as follows:

(1) If the primary star becomes a red giant (case C evolution), it then undergoes the second dredge-up, forming a thin He layer as seen in Figure 1, and enters the AGB phase. The C+O core mass, $M_{\rm CO}$, at this phase is larger for more massive stars. For a larger $M_{\rm CO}$ the total carbon mass fraction is smaller. When it enters the AGB phase, the star greatly expands and is assumed here to undergo Roche lobe overflow (or a super-wind phase) and to form a C+O WD. Thus the initial mass of the WD, $M_{\rm WD,0}$, at the beginning of mass accretion is approximately equal to $M_{\rm CO}$.

(2) If the primary star becomes a He star (case BB evolution), the second dredge-up in case C corresponds to the expansion of the He envelope even to a red-giant size. The ensuing Roche lobe overflow of the He envelope leads to a white dwarf of mass $M_{\rm WD,0} = M_{\rm CO}$.

https://doi.org/10.1017/S0074180900113725 Published online by Cambridge University Press

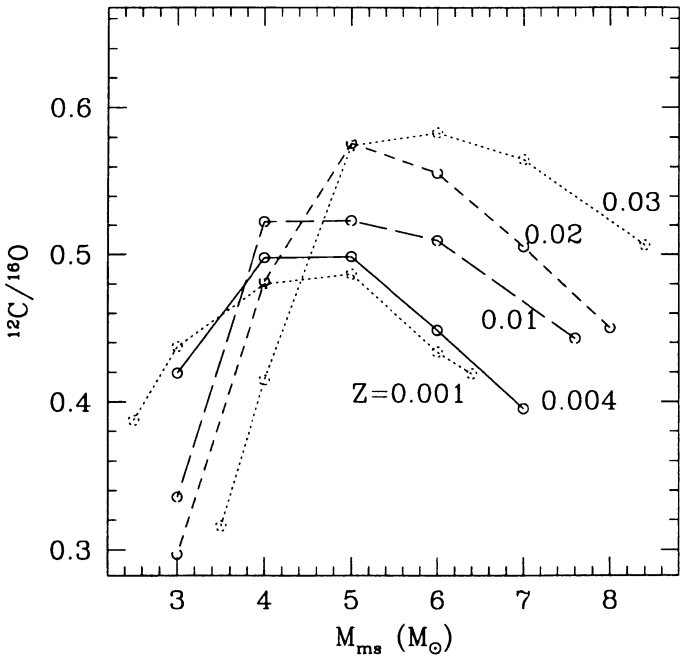

Figure 2. The central C/O ratio in mass fraction as a function of metallicity and stellar mass (Umeda et al. 1998).

(3) After the onset of mass accretion, the WD mass grows through steady H burning and weak He shell flashes. The composition of the growing C+O layer can be approximated as C/O = 1. The WD grows in mass and ignites carbon when its mass reaches $M_{\rm Ia} = 1.378 M_\odot$ (Nomoto et al. 1984).

Figure 3 shows the metallicity dependence of the relation between the ZAMS mass ($M_{\rm ms}$) and $M_{\rm CO} = M_{\rm WD,0}$. We note that stars with higher metallicity form smaller C-O cores if they have the same $M_{\rm ms}$.

The WD mass at the onset of mass transfer from the companion star ($M_{\rm WD,0}$) is critically important for the fate of the accreting WD. For $M_{\rm WD,0}$ as low as $\lesssim 0.7 M_\odot$, the WD mass is difficult to reach $M_{\rm Ia} \simeq 1.37 - 1.38 M_\odot$, unless the companion star is massive (and thus young) enough to supply the required amount of mass. For higher $M_{\rm WD,0}$, the WD can become SNe Ia even with a small mass (and thus long-lived) companion.

Figure 4 shows the total mass of ^{12}C ($M(^{12}{\rm C})$) integrated over the WD mass, $M_{\rm Ia} = 1.378 M_\odot$, just before the SN Ia explosion. Here we assume C/O $\sim$ 1 in the outer layer of $M_{\rm CO} \leq M_r \leq M_{\rm Ia}$ which is formed by He shell burning during accretion. If $M(^{12}{\rm C})$ is plotted against $M_{\rm WD,0} = M_{\rm CO}$ rather than $M_{\rm ms}$, the curves for different metallicity are very similar. The total carbon mass fraction just before SN Ia explosion is seen to vary in

https://doi.org/10.1017/S0074180900113725 Published online by Cambridge University Press

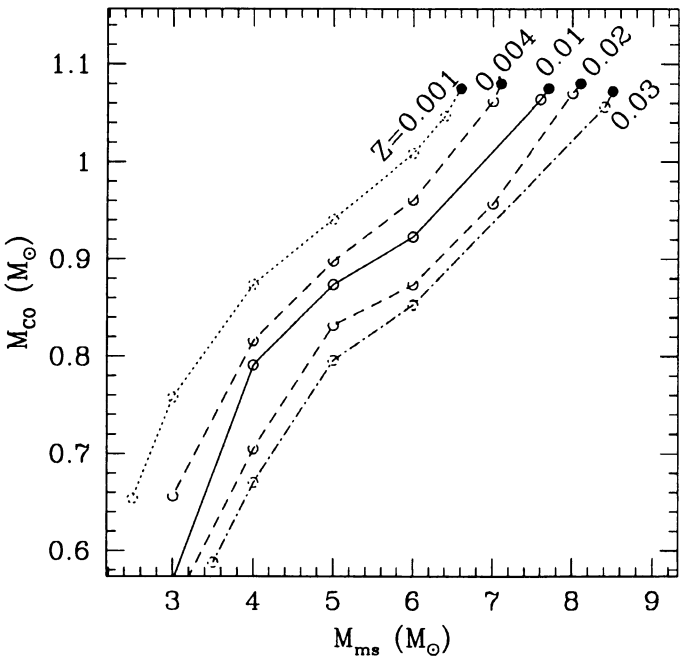

Figure 3. Metallicity dependence of the ZAMS mass ($M_{\rm ms}$) vs. C-O core mass ($M_{\rm CO}$) at the end of the second dredge-up. Filled circles indicate that off-center carbon ignition occurs in these model. Hence, the abscissa of these points correspond to the $M_{\rm UP}$ (Umeda et al. 1998).

the range $M(^{12}{\rm C})/M_{\rm Ia} = 0.3 - 0.5$.

Such a variation of $M(^{12}{\rm C})/M_{\rm Ia}$ may be partially responsible for the observed variations in the brightness and spectra of SNe Ia. Most of previous works on the SNe Ia explosion have used progenitor models with C/O = 1. Only recently Höflich et al. (1998) have started investigation of different C/O for the DD models. The variation of C/O ratio would be important, if it affects the ρ_{tr} in the DD model to induce a large variation in the explosion energy.

The ranges of the variation in the central C/O ratio and $M(^{12}{\rm C})/M_{\rm Ia}$ obtained above do not significantly depend on Z for $0.001 \leq Z \leq 0.02$. These ratios exhibit smaller dispersion with respect to metallicity if these ratios are plotted against $M_{\rm CO}$ (Fig. 4). Moreover, WDs with $Z \lesssim 0.002$ need not be considered for SNe Ia progenitors, because such low metallicity WDs blow too weak winds to evolve into SNe Ia as will be discussed in §4. In this sense, the metallicity effects are relatively minor for the same $M_{\rm CO}$. These would be good for determining cosmological parameters with the use of SNe Ia, because "evolutionary" effects on the SN Ia properties are minor at different red-shifts.

https://doi.org/10.1017/S0074180900113725 Published online by Cambridge University Press

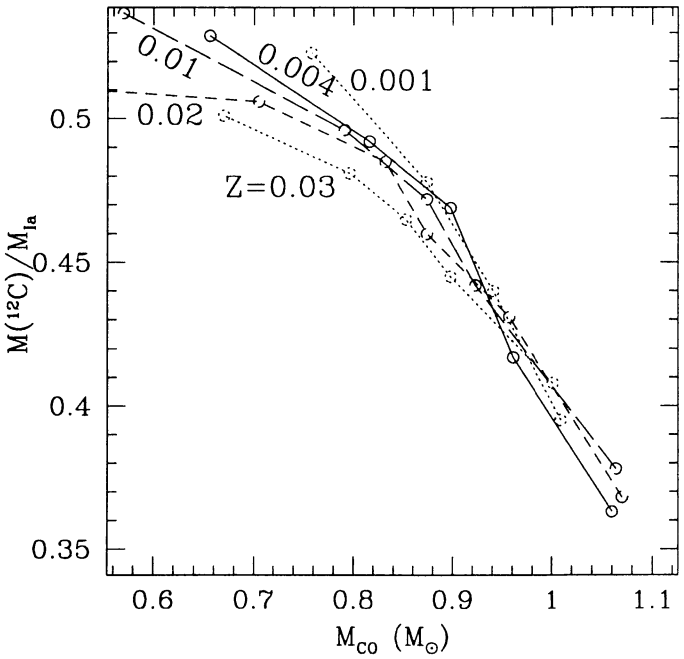

Figure 4. Total ^{12}C mass ($M(^{12}\mathrm{C})$) included in the WD of mass $M_{\mathrm{Ia}} = 1.37M_{\odot}$ just before an SN Ia explosion as a function of M_{CO} (Umeda et al. 1998).

3. Progenitors of Type Ia Supernovae

The progenitors of the majority of SNe Ia are most likely the Chandrasekhar (Ch) mass WDs, although the sub-Ch mass models might correspond to some peculiar subluminous SNe Ia (e.g., Nomoto et al. 1997ab). For the evolution of accreting WDs toward the Ch mass, two scenarios have been proposed: One is a double-degenerate (DD) scenario, i.e., merging of double C+O WDs with a combined mass surpassing the Ch mass limit (Iben & Tutukov 1984; Webbink 1984), and the other is a single-degenerate (SD) scenario, i.e., accretion of hydrogen-rich matter via mass transfer from a binary companion (e.g., Nomoto 1982). Though the issue of DD versus SD is still debated, theoretical modeling has indicated that the merging of WDs leads to the collapse to form a neutron star rather than SNe Ia (Nomoto & Kondo 1991).

For the SD scenario, a new evolutionary model has been proposed by Hachisu, Kato, & Nomoto (1996, 1998; hereafter HKN96 and HKN98, respectively). HKN96 have shown that if the accretion rate exceeds a certain limit, the WD blows a strong wind and burns hydrogen steadily to increase the WD mass to M_{Ia}. HKN98 have further invoked the effect of stripping-off of the envelope from the companion by the strong wind, which stabilizes

https://doi.org/10.1017/S0074180900113725 Published online by Cambridge University Press

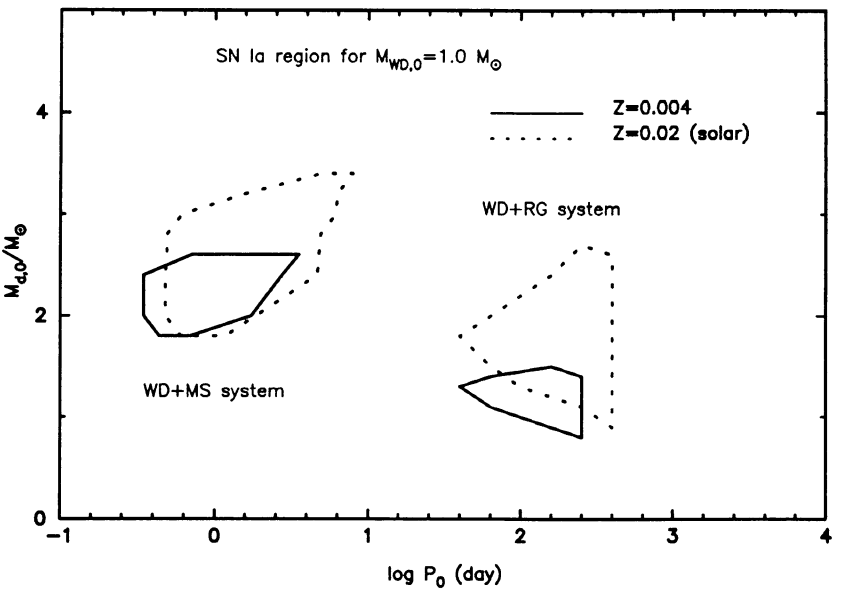

Figure 5. The regions of SNe Ia is plotted in the initial orbital period vs. the initial companion mass diagram for the initial WD mass of $M_{\rm WD,0} = 1.0 M_\odot$. The dashed and solid lines represent the cases of solar abundance ($Z = 0.02$) and much lower metallicity of $Z = 0.004$, respectively. The left and the right regions correspond to the WD+MS and the WD+RG systems, respectively (Kobayashi et al. 1998).

the mass transfer and prevents the system from forming a common envelope. Thus the WD can reach the Ch mass for much wider binary parameter space than found by HKN96, Li & van den Heuvel (1997), and Yungelson & Livio (1998); the allowed parameter space may be large enough to account for the SN Ia frequency.

There are two cases of the companion star: One is a red-giant (RG) with an initial mass of $M_{\rm RG,0} \sim 1 M_\odot$ and an orbital period of tens to hundreds days (HKN96, HKN98), the other is a near main-sequence (MS) with an initial mass of $M_{\rm MS,0} \sim 2 - 3 M_\odot$ and a period of several tenths of a day to several days (Li & van den Heuvel 1997; HKN98).

Figure 5 shows the SN Ia regions in the diagram of the initial orbital period vs. the initial mass of the companion star for the initial WD mass of $M_{\rm WD,0} = 1.0 M_\odot$. In these regions, the accretion from the companion star increases the WD mass successfully through the occurrence of SN Ia. The dashed line shows the case of solar abundance ($Z = 0.02$), while the solid line shows the much lower metallicity case of $Z = 0.004$; the metallicity dependence will be discussed in the next section.

https://doi.org/10.1017/S0074180900113725 Published online by Cambridge University Press

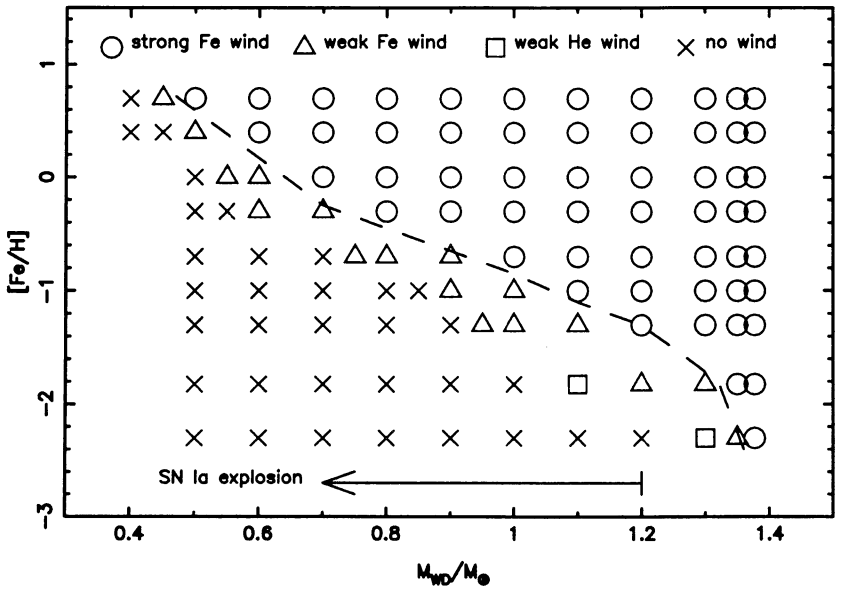

Figure 6. WD mass vs. metallicity diagram showing the metallicity dependence of optically thick winds. The wind is regarded as "strong" if the wind velocity at the photosphere exceeds the escape velocity but "weak" if the wind velocity is lower than the escape velocity. The term of "He" or "Fe" wind denotes that the wind is accelerated by the peak of iron lines near $\log T(\mathrm{K}) \sim 5.2$ or of helium lines near $\log T(\mathrm{K}) \sim 4.6$. The dashed line indicates the demarcation between the "strong" wind and the "weak" wind (Kobayashi et al. 1998).

4. Low-Metallicity Inhibition of Type Ia Supernovae

The white dwarf wind model introduces an important metallicity effect as noted in Kobayashi et al. (1998). The optically thick winds are driven by a strong peak of OPAL opacity at $\log T(\mathrm{K}) \sim 5.2$ (Iglesias & Rogers 1993). Since the peak is due to iron lines, the optically thick winds depend strongly on the metallicity. If the iron abundance of the accreted matter is as low as $[\mathrm{Fe/H}] \lesssim -1$, the WD wind is too weak to increase the WD mass through the Ch mass.

Figure 6 shows the metallicity dependence of the optically thick winds. The strong winds are possible only for the region above the dashed line. The term "weak" implies that the wind velocity at the photosphere does not exceed the escape velocity there, that is, it cannot blow the accreted matter off the WD. For the metallicity as small as $Z = 0.001$, the opacity peak at $\log T \sim 5.2$ is very weak, being smaller than the peak of helium lines at $\log T \sim 4.6$. Then, the wind is driven by the helium line peak rather

https://doi.org/10.1017/S0074180900113725 Published online by Cambridge University Press

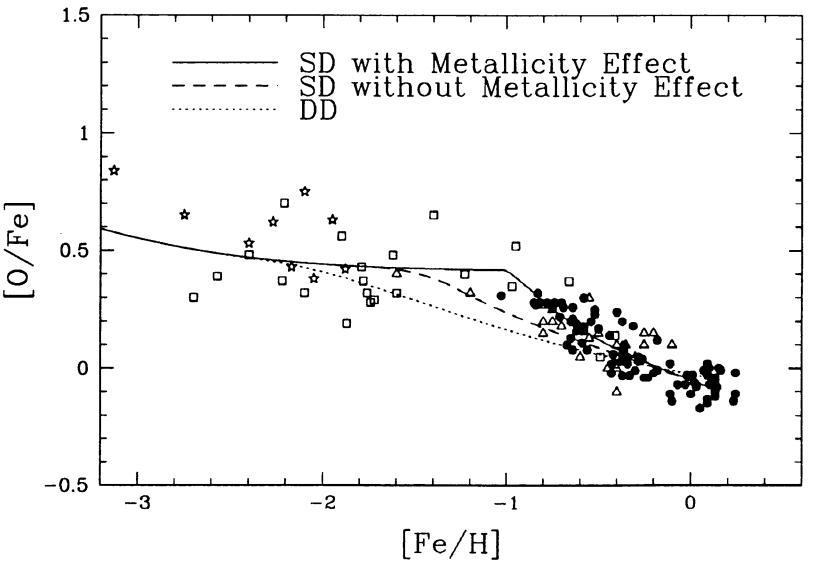

Figure 7. The evolutionary change in [O/Fe] against [Fe/H] for three SN Ia models (Kobayashi et al. 1998). The dotted line is for the DD scenario, and the other lines are for our SD scenario with (solid line) and without (dashed line) the metallicity effect on SNe Ia. Observational data sources: filled circles, (Edvardson et al. 1993); open triangles, (Barbuy et al. 1989); stars, (Nissen et al. 1994); open squares, (Gratton et al. 1991).

than the iron line peak, which we call "He wind" instead of "Fe wind". Since only the initial WD mass of $M_{\rm WD,0} \leq 1.2M_\odot$ can produce an SN Ia (Nomoto & Kondo 1991), SN Ia events occur only for the progenitors with [Fe/H] $\gtrsim -1.1$, which is adopted in our chemical evolution model.

The size of SN Ia regions in Figure 5 clearly demonstrate the metallicity effect, i.e., SN Ia regions are much smaller for smaller metallicity. The initial mass ranges of the companion stars for $Z = 0.004$ are $0.9M_\odot \lesssim M_{\rm RG,0} \lesssim 1.5M_\odot$ for the WD+RG system and $1.8M_\odot \lesssim M_{\rm MS,0} \lesssim 2.6M_\odot$ for the WD+MS system.

5. The Chemical Evolution in the Solar Neighborhood

The role of SNe II and SNe Ia in the chemical evolution of galaxies can be seen in the [O/Fe]-[Fe/H] relation (Fig. 7: Metal-poor stars with [Fe/H] $\lesssim -1$ have [O/Fe] ~ 0.45 on the average, while disk stars with [Fe/H] $\gtrsim -1$ show a decrease in [O/Fe] with increasing metallicity. To explain such an evolutionary change in [O/Fe] against [Fe/H], we use the chemical evolution model that allows the infall of material from outside the disk region. The infall rate, the SFR, and the initial mass function (IMF) are

https://doi.org/10.1017/S0074180900113725 Published online by Cambridge University Press

given by Kobayashi et al. (1998), and the nucleosynthesis yields of SNe Ia and II are taken from Tsujimoto et al. (1995).

For the SD scenario, the lifetime of SNe Ia is determined from the main-sequence lifetime of the companion star. The initial mass ranges of the companions are $0.9M_\odot \lesssim M_{\rm RG,0} \lesssim 1.5M_\odot$ for the WD+RG system and $1.8M_\odot \lesssim M_{\rm MS,0} \lesssim 2.6M_\odot$ for the WD+MS system. The low-metallicity inhibition of SNe Ia is introduced for the metallicity of the progenitor systems lower than [Fe/H]$= -1.1$, which is determined from the metallicity dependence of the optically thick wind. For the DD scenario, we adopt the distribution function of the lifetime of SNe Ia by Tutukov & Yungelson (1994), majority of which is $\sim 0.1 - 0.3$ Gyr.

Figure 7 shows the evolutionary change in [O/Fe] for three SN Ia models. The dotted line is for the DD scenario. The other lines are for our SD scenario with (solid line) and without (dashed line) the metallicity effect on SNe Ia. i) In the DD scenario the lifetime of the majority of SNe Ia is shorter than 0.3 Gyr. Then the decrease in [O/Fe] starts at [Fe/H] ~ -2, which is too early compared with the observed decrease in [O/Fe] starting at [Fe/H] ~ -1. ii) For the SD scenario with no metallicity effect, the companion star with $M \sim 2.6M_\odot$ evolves off the main-sequence to give rise to SNe Ia at the age of ~ 0.6 Gyr. The resultant decrease in [O/Fe] starts too early to be compatible with the observations. iii) For the metallicity dependent SD scenario, SNe Ia occur at [Fe/H] $\gtrsim -1$, which naturally reproduce the observed break in [O/Fe] at [Fe/H] ~ -1.

6. Galactic Halo and damped Lyα systems

The low-metallicity inhibition of SNe Ia can provide a new interpretation of the SN II-like abundance patterns:

1) The Galactic halo is a low-metallicity system with [Fe/H] $\lesssim -1$, and it has an abundance pattern of genuine SN II origin, i.e., the overabundances of α-elements relative to Fe as [α/Fe] > 0 (Wheeler, Sneden & Truran 1989). However there exist age differences of several Gyrs among the clusters as well as field stars. Since the shortest lifetime of SNe Ia is ~ 0.6 Gyr for the MS+WD close binary systems, SN Ia contamination would be seen in [α/Fe] if there were no metallicity effect on SNe Ia. This apparent discrepancy between the age difference and the high [α/Fe] can be resolved by the low-metallicity inhibition of SNe Ia.

2) A similar interpretation also holds for DLA systems. The DLA systems observed at $0.7 < z < 4.4$ have [Fe/H]$= -2.5$ to -1 and indicate [α/Fe] > 0 (Lu et al. 1996). The age-metallicity relation in DLA systems suggested by Lu et al. (1996) implies that DLA systems have grown through a common chemical history spanning over several Gyrs. If so, the SN II-like abundance

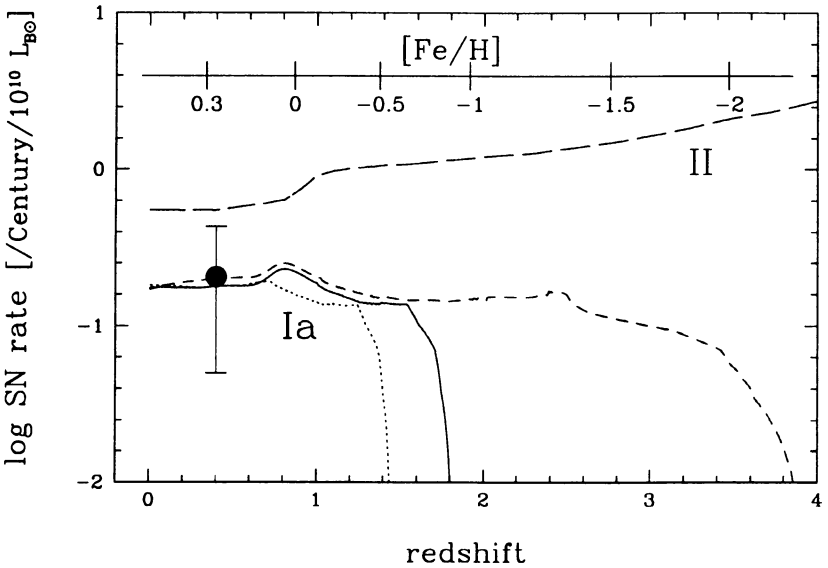

Figure 8. The cosmic supernova rate per $10^{10}L_{\odot}$ per century (SNu). The long-dashed line is for SNe II and the other lines for SNe Ia with (solid and dotted lines) and without (dashed line) the metallicity effect. The correction of the dust extinction is included in the SFR (Pettini et al. 1998) except for the dotted line which shows the SN Ia rate without this correction (Madau et al. 1996). The filled circle is the observed SN Ia rate at $z \sim 0.4$ (Pain et al. 1996). The iron-abundance scale in the abscissa is calculated with the metallicity effect on SNe Ia.

pattern in DLA systems needs the introduction of the metallicity dependent SN Ia rate to avoid the contamination of SN Ia products.

7. Cosmic Supernovae Rate

SNe Ia have been discovered up to $z \sim 1.2$ by the Supernova Cosmology Project and the High-z Supernova Search Team. They have given the SN Ia rate at $z \sim 0.4$ (Pain et al. 1996) but will provide the SN Ia rate history over $0 < z < 1.3$. With the Next Generation Space Telescope, both SNe Ia and II will be observed through $z \sim 4$. In a theoretical approach, the cosmic SN Ia rate as a function of redshift has been constructed for a cosmic star formation rate (SFR). In this paper, we make a prediction of the cosmic SN Ia rate as a composite of different types of galaxies which have gone through different chemical enrichment.

First, we predict the cosmic supernova rate history corresponding to the observed cosmic SFR (e.g., Madau et al. 1996) with the correction of the dust extinction (Pettini et al. 1998). The photometric evolution is calculated with the spectral synthesis population database taken from Kodama &

https://doi.org/10.1017/S0074180900113725 Published online by Cambridge University Press

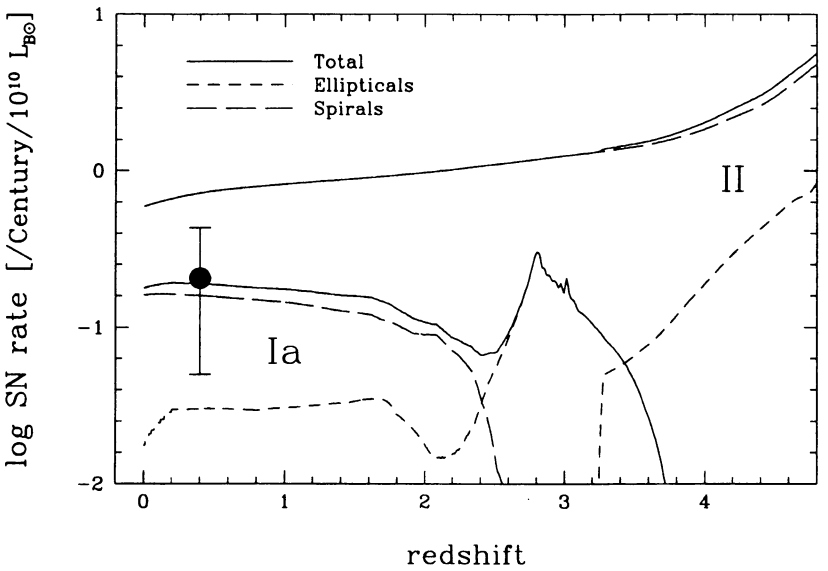

Figure 9. The cosmic supernovae rate in SNu as a composite of ellipticals and spirals. The upper three lines show SN II rates, the lower three lines show SN Ia rates. The solid-line, the short dashed-line, and the long dashed-line are for total, ellipticals, and spirals, respectively.

Arimoto (1997). We adopt $H_0 = 50$ km s^{-1} Mpc^{-1}, $\Omega_0 = 0.2$, $\lambda_0 = 0$, and the redshift at the formation epoch of galaxies $z_f = 5$. We determine the initial comoving density of gas $\Omega_{g\infty}$ to reproduce the present gas fraction $\Omega_{g0} = 5 \times 10^{-4}$.

Figure 8 shows the cosmic supernova rate per $10^{10} L_\odot$ per century (SNu). The long-dashed line is for SNe II and the other lines for SNe Ia with (solid and dotted lines) and without (dashed line) the metallicity effect. The dotted line shows the SN Ia rate without the correction of the dust extinction in the SFR (Madau et al. 1996).

If we do not include the metallicity effect, the SN Ia rate is almost flat from the present to higher redshift, and decreases toward the formation epoch of galaxies. If we include the metallicity effect, the SN Ia rate drops at $z \sim 1.4 - 1.8$, where the iron abundance of the gas in the universe is too low (i.e., [Fe/H] $\lesssim -1$) for the progenitors of SNe Ia to make explosions. The redshift where the SN Ia rate drops is determined by the speed of the chemical enrichment, which depends on the effect of dust extinction on the cosmic SFR, cosmology, galaxy formation epoch, and the initial gas density. Taking into account these uncertainties, the break in the SN Ia rate occurs at $z = 1 - 2$.

In fact, galaxies being responsible for the cosmic SFR have different

https://doi.org/10.1017/S0074180900113725 Published online by Cambridge University Press

heavy-element enrichment timescale, so that we calculate the cosmic chemical evolution as a composite of ellipticals and spirals (S0a-Sa, Sab-Sb, Sbc-Sc, and Scd-Sd). We assume that elliptical galaxies are formed by a single star burst and stop the star formation after the supernova-driven galactic wind (Kodama & Arimoto 1997), while spiral galaxies are formed by a relatively continuous star formation. The epoch of the end of star formation in ellipticals is assumed to be 1 Gyr, which correspond to the redshift of $z \sim 3$. The infall rate and the SFR are given by Kobayashi et al. (1998). We then combine the contribution of ellipticals and spirals with the relative mass ratio among the types. The predicted cosmic SFR have the little smaller slope than the observed cosmic SFR from the present to the peak at $z \sim 1.4$ and the excess at $z \gtrsim 2$ corresponding to the SFR of ellipticals which may be hidden by the dust extinction.

Figure 9 shows the cosmic supernova rate (solid-line) as the composite of ellipticals (short dashed-line) and spirals (long dashed-line). The upper three lines show the SN II rates and the lower three lines show the SN Ia rates. The SN Ia rate in spirals decreases at $z \sim 2.5$ because of the low-metallicity inhibition of SNe Ia. We can find many SNe Ia at $z > 3$ in ellipticals, where the chemical enrichment takes place so early that the metallicity effect on SN Ia is not effective.

8. Discussion

We discuss the metallicity effects on the properties of the SN Ia progenitors such as the C/O ratio in the WDs. We introduce a metallicity dependence of the SN Ia rate in the Galactic and cosmic chemical evolution models. In this scenario involving a strong wind from WDs, few SNe Ia occur at [Fe/H] $\lesssim -1$. This model successfully reproduces the observed chemical evolution in the solar neighborhood. Following predictions can be made as a test of these metallicity effects.

i) SNe Ia are not found in the low iron abundance environments such as dwarf galaxies and the outskirts of spirals.

ii) The cosmic SN Ia rate drops at $z \sim 1-2$ because of the low-iron abundance, which can be observed with the Next Generation Space Telescope.

iii) At $z > 3$, SNe Ia can be found in ellipticals where the timescale of metal enrichment is sufficiently short, while the SN Ia rate in spirals drops at $z \sim 2.5$ due to the low-iron abundance.

This work has been supported in part by the grant-in-Aid for COE Scientific Research (07CE2002) of the Japanese Ministry of Education, Science, Sports, and Culture.

References

Arnett, W.D. 1996, Nucleosynthesis and Supernovae (Princeton: Princeton Univ. Press)
Barbuy, B., & Erdelyi-Mendes, M. 1989, A&A 214, 239
Branch, D. 1998, ARA&A 36, 17
Edvardsson, B. et al. 1993, A&A 275, 101
Gratton, R. G. 1991, in IAU Symp. 145, Evolution of Stars: The Photometric Abundance Connection, ed. G. Michaud & A. V. Tutukov (Montreal: Univ. Montreal), 27
Hachisu, I., Kato, M., & Nomoto, K. 1996, ApJ 470, L97 (HKN96)
Hachisu, I., Kato, M., & Nomoto, K. 1998, ApJ, submitted (HKN98)
Höflich, P., Wheeler, J. C., & Thielemann, F. -K., 1998, ApJ 495, 617
Iben, I. Jr., & Tutukov, A. V. 1984, ApJ-S 54, 335
Iglesias, C. A., & Rogers, F. 1993, ApJ 412, 752
Kobayashi, C., Tsujimoto, T., Nomoto, K., Hachisu, I, & Kato, M. 1998, ApJ 503, L155
Kodama, T., & Arimoto, N. 1997, A&A 320, 41
Li, X. -D., & van den Heuvel, E. P. J. 1997, A&A 322, L9
Lu, L., Sargent, W. L. W., Barlow, T. A., Churchill, C. W., & Vogt, S. S. 1996, ApJS 107, 475
Madau, P., Ferguson, H. C., Dickinson, M. E., Giavalisco, M., Steidel, C. C., & Fruchter, A. 1996, MNRAS 283, 1388
Nissen, P. E., Gustafsson, B., Edvardsson, B., & Gilmore, G. 1994, A&A 285, 440
Nomoto, K., 1982, ApJ 253, 798
Nomoto, K., Iwamoto, K., & Kishimoto, N. 1997a, Science 276, 1378
Nomoto, K., Iwamoto, K., et al. 1997b, in Thermonuclear Supernovae, Eds. P.Ruiz-Lapuente et al. (Dordrecht: Kluwer), 349
Nomoto, K., & Kondo, Y. 1991, ApJ 367, L19
Nomoto, K., Thielemann, F. -K., & Yokoi, K., 1984, ApJ, 286, 644
Nomoto, K., Yamaoka, H., Shigeyama, T., Kumagai, S., & Tsujimoto, T. 1994, in Supernovae, Les Houches Session LIV, ed. S. A. Bludman et al. (Amsterdam: North-Holland), 199
Pain, R., et al. 1996, ApJ 473, 356
Perlmutter, S., et al. 1997, ApJ 483, 565
Pettini, M., Kellogg, M.,Steidel, C.,Dickinson, M., Adelberger, K. L, & Giavalisco, M. 1998, ApJ 508, 539
Phillips, M. M. 1993, ApJ 413, L75
Riess, A.G., Press, W.H., & Kirshner, R.P. 1995, ApJ 438, L17
Ruiz-Lapuente, P., Canal, R., & Isern, J., eds. 1997, "Thermonuclear Supernovae" (Dordrecht: Kluwer)
Schmidt, B. et al. 1998, ApJ 507, 46
Tsujimoto, T., Nomoto, K., Yoshii, Y., Hashimoto, M., Yanagida, S., & Thielemann, F.-K. 1995, MNRAS 277, 945
Tutukov, A. V., & Yungelson, L. R. 1994, MNRAS 268, 871
Umeda, H., Nomoto, K., Yamaoka, H., & Wanajo, S. 1998, ApJ, in press
Webbink, R. F. 1984, ApJ 277, 355
Wheeler, J. C., Sneden, C., & Truran, J. W. 1989, ARA&A 27, 279
Yungelson, L., & Livio, M. 1998, ApJ 497, 168